

Polarized neutron scattering studies of magnetic excitations in electron-overdoped superconducting $\text{BaFe}_{1.85}\text{Ni}_{0.15}\text{As}_2$

Mengshu Liu,¹ C. Lester,² Jiri Kulda,³ Xinye Lu,^{4,1} Huiqian Luo,⁴ Meng Wang,⁴ Stephen M. Hayden,² and Pengcheng Dai^{1,4}

¹ *Department of Physics and Astronomy, The University of Tennessee, Knoxville, Tennessee 37996-1200, USA*

² *H. H. Wills Physics Laboratory, University of Bristol, Tyndall Avenue, Bristol, BS8 1TL, UK*

³ *Institut Laue-Langevin, 6, rue Jules Horowitz, BP 156, 38042 Grenoble Cedex 9, France*

⁴ *Beijing National Laboratory for Condensed Matter Physics, Institute of Physics, Chinese Academy of Sciences, Beijing 100190, China*

(Dated: March 4, 2013)

We use polarized inelastic neutron scattering to study low-energy spin excitations and their spatial anisotropy in electron-overdoped superconducting $\text{BaFe}_{1.85}\text{Ni}_{0.15}\text{As}_2$ ($T_c = 14$ K). In the normal state, the imaginary part of the dynamic susceptibility, $\chi''(Q, \omega)$, at the antiferromagnetic (AF) wave vector $Q = (0.5, 0.5, 1)$ increases linearly with energy for $E \leq 13$ meV. Upon entering the superconducting state, a spin gap opens below $E \approx 3$ meV and a broad neutron spin resonance appears at $E \approx 7$ meV. Our careful neutron polarization analysis reveals that $\chi''(Q, \omega)$ is isotropic for the in-plane and out-of-plane components in both the normal and superconducting states. A comparison of these results with those of undoped BaFe_2As_2 and optimally electron-doped $\text{BaFe}_{1.9}\text{Ni}_{0.1}\text{As}_2$ ($T_c = 20$ K) suggests that the spin anisotropy observed in $\text{BaFe}_{1.9}\text{Ni}_{0.1}\text{As}_2$ is likely due to its proximity to the undoped BaFe_2As_2 . Therefore, the neutron spin resonance is isotropic in the overdoped regime, consistent with a singlet to triplet excitation.

PACS numbers: 74.70.Xa, 75.30.Gw, 78.70.Nx

I. INTRODUCTION

Understanding the role of spin excitations in the superconductivity of iron arsenides¹⁻³ is important for developing a microscopic theory of superconductivity in these materials⁴⁻⁸. Like copper oxide superconductors, superconductivity in iron pnictides arises when electrons or holes are doped into their antiferromagnetically-ordered parent compounds⁹. For electron-doped $\text{BaFe}_{2-x}\text{TxAs}_2$ ($T = \text{Co, Ni}$)³, the antiferromagnetic (AF) and superconducting phase diagrams as a function of Co(Ni)-doping have been determined by neutron scattering experiments (Fig. 1(a))^{10,11}. Near the optimally electron-doped superconductor $\text{BaFe}_{2-x}\text{Ni}_x\text{As}_2$ at $x = 0.1$ ($T_c = 20$ K), the static AF order is suppressed¹². However, short-range spin excitations persist and couple directly to superconductivity via a collective magnetic excitation termed the neutron spin resonance¹²⁻¹⁷. As a function of Ni-doping, the energy of the resonance is associated with both the superconducting electronic gap Δ and $k_B T_c$, thus indicating its direct connection with superconductivity¹⁸.

Although the resonance appears to be a common feature amongst different classes of unconventional superconductors including high- T_c copper oxides¹⁹⁻²³, heavy Fermions^{24,25}, and iron-based materials^{12-17,26-28}, much remains unknown about its microscopic origin. Assuming that the resonance is a spin-1 singlet-to-triplet excitation of the Cooper pairs²⁹, it should be possible to split it into three peaks under the influence of a magnetic field via the Zeeman effect by an amount $\Delta E = \pm g\mu_B B$, where $g = 2$ is the Lande factor and B is the magnitude of the field³⁰⁻³³. Although there have been attempts to split the resonance for copper oxide³⁰ and iron-based

superconductors^{31,32} in this way, the results are inconclusive and it has not been possible to determine if the mode is indeed a singlet-to-triplet excitation. In a very recent neutron experiment performed on the heavy Fermion superconductor CeCoIn_5 , the resonance was shown to be a doublet excitation³³, thus casting doubt on its direct connection with superconducting Cooper pairs³⁴.

Alternatively, one can use neutron polarization analysis to determine the nature of the resonance and the effect of superconductivity on spin excitations. If the resonance is an isotropic triplet excitation of the singlet superconducting ground state, one expects that the degenerate triplet would be isotropic in space. Utilising neutron polarization analysis, one can conclusively separate the magnetic signal from lattice scattering and determine the spatial anisotropy of the magnetic excitations³⁵. For the optimally hole-doped copper oxide superconductor $\text{YBa}_2\text{Cu}_3\text{O}_{6.9}$ ¹⁹⁻²², recent polarized neutron scattering experiments reveal that while the resonance at $E = 41$ meV is isotropic in space, magnetic excitations below the resonance ($10 \leq E \leq 30$ meV) exhibit large anisotropy with the excitations polarized along the c -axis being suppressed³⁶. These results suggest that while the resonance itself is consistent with a spin-1 singlet-to-triplet excitation, the emergence of low-energy spin anisotropy may arise from the spin-orbit coupling due to the Dzyaloshinskii-Moriya interactions between the copper spins³⁷. In the case of iron-based superconductors, the situation is more complicated. For optimally electron-doped $\text{BaFe}_{1.9}\text{Ni}_{0.1}\text{As}_2$, polarized neutron scattering experiments indicate that while the magnetic scattering is essentially isotropic in the normal state, a large spin anisotropy develops below T_c . Excitations polarized

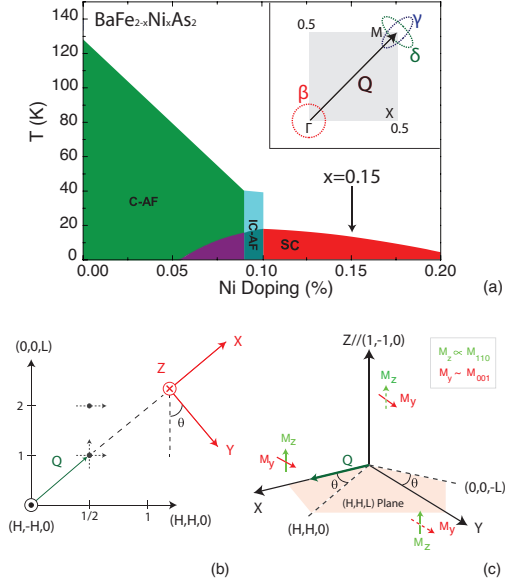


FIG. 1: (Color online) (a) The schematic antiferromagnetic and superconducting phase diagram of $\text{BaFe}_{2-x}\text{Ni}_x\text{As}_2$ as determined from neutron diffraction experiments¹¹. The present composition is highlighted with an arrow. The inset shows an illustration of quasiparticle excitations from the hole Fermi pocket at the Γ point to the electron pocket at the M point as predicted by Fermi surface nesting theories. (b) The three neutron polarization directions (x , y and z) oriented in the (H, H, L) plane of the reciprocal space. (c) The relationship between magnetic components M_y and M_z measured by polarized neutron scattering and in-plane (M_{110}) and out-of-plane (M_{001}) dynamic spin susceptibility. The solid arrow denotes the measured magnetic component in a SF channel and the dashed arrow denotes the component measured in a NSF channel. In this geometry, we have $M_z \propto M_{110} = M_{110}$, due to tetragonal symmetry; and $M_y \sim M_{001}$, given that θ is a small value.

along the c -axis are larger than those in the plane for energies $2 \leq E \leq 6$ meV, i.e. below the weakly anisotropic resonance³⁸. On the other hand, similar measurements on superconducting $\text{FeSe}_{0.5}\text{Te}_{0.5}$ reveal an anisotropic resonance with the in-plane component slightly larger than the out-of-plane component³⁹. However, the spin excitations are isotropic for energies below and above the resonance³⁹. Finally, recent neutron polarization analysis of spin waves in the undoped AF BaFe_2As_2 ⁴⁰ indicate that the magnetic single-ion anisotropy induced spin-wave gaps^{41,42} are strongly anisotropic, with the in-plane component of the spin-wave gap much larger than that of the c -axis component. Therefore, it costs more energy to rotate a spin within the orthorhombic a - b plane than rotating it perpendicular to the FeAs layers in the AF ordered state of BaFe_2As_2 ⁴⁰.

Given the current confusing experimental situation on the anisotropy of spin excitations in undoped and optimally electron-doped $\text{BaFe}_{2-x}\text{Ni}_x\text{As}_2$ ^{38,40}, it would be interesting to carry out similar polarized neutron scattering measurements for electron overdoped

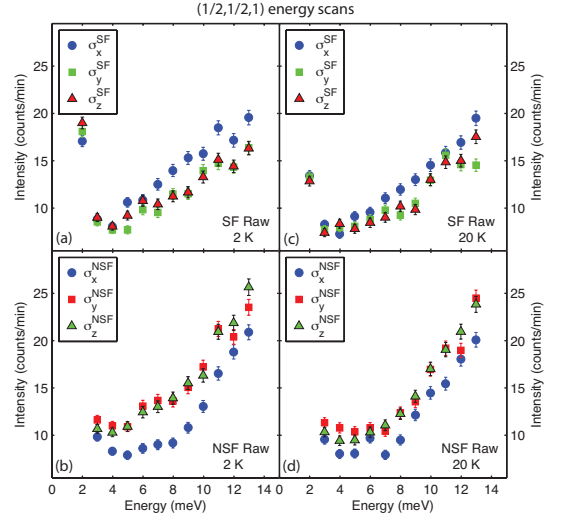


FIG. 2: (Color online) Constant- Q scans at $\mathbf{Q} = (0.5, 0.5, 1)$ below and above T_c . Using polarized neutrons, we can measure six independent scattering cross sections: incoming neutrons polarized along the x , y or z directions, with outgoing neutrons flipped (SF), or not flipped (NSF). (a) The raw data for SF scattering at 2 K, denoted as $\sigma_{x,y,z}^{\text{SF}}$; (b) Identical scans in NSF channel, or $\sigma_{x,y,z}^{\text{NSF}}$; (c) SF scattering $\sigma_{x,y,z}^{\text{SF}}$ at 20 K, and (d) NSF scattering $\sigma_{x,y,z}^{\text{NSF}}$ at 20 K.

$\text{BaFe}_{2-x}\text{Ni}_x\text{As}_2$. From the electronic phase diagram of $\text{BaFe}_{2-x}\text{Ni}_x\text{As}_2$ in Fig. 1(a)¹¹, we see that samples in the overdoped regime are far from the AF and superconductivity co-existence region, and thus avoid possible influence of the local magnetic anisotropy present in undoped BaFe_2As_2 ⁴⁰. For our neutron experiments, we prepared over-doped $\text{BaFe}_{1.85}\text{Ni}_{0.15}\text{As}_2$ with $T_c = 14$ K (Fig. 1(a)). In this article, we describe polarized neutron scattering studies of energy and momentum dependence of the magnetic excitations in $\text{BaFe}_{1.85}\text{Ni}_{0.15}\text{As}_2$ below and above T_c . We find that the spin excitations at or near the resonance energy are spatially isotropic. By comparing these results with previous work on undoped BaFe_2As_2 and optimally doped $\text{BaFe}_{1.9}\text{Ni}_{0.1}\text{As}_2$ ^{38,40}, we conclude that the strong in-plane single-ion anisotropy in antiferromagnetically-ordered orthorhombic BaFe_2As_2 extends to the paramagnetic tetragonal $\text{BaFe}_{1.9}\text{Ni}_{0.1}\text{As}_2$, giving rise to the large out-of-plane component of the low-energy spin excitations for the superconducting $\text{BaFe}_{1.9}\text{Ni}_{0.1}\text{As}_2$. Therefore, the resonance in optimally and overdoped $\text{BaFe}_{2-x}\text{Ni}_x\text{As}_2$ ($x = 0.1, 0.15$) is mostly isotropic in space, consistent with the singlet-to-triplet excitation scenario.

II. EXPERIMENTAL DETAILS

We grew large single crystals of the overdoped iron arsenide superconductor $\text{BaFe}_{1.85}\text{Ni}_{0.15}\text{As}_2$ using a self-flux method⁴³. $\text{BaFe}_{1.85}\text{Ni}_{0.15}\text{As}_2$ has a T_c of 14 K, and is far away from the AF phase of the undoped BaFe_2As_2

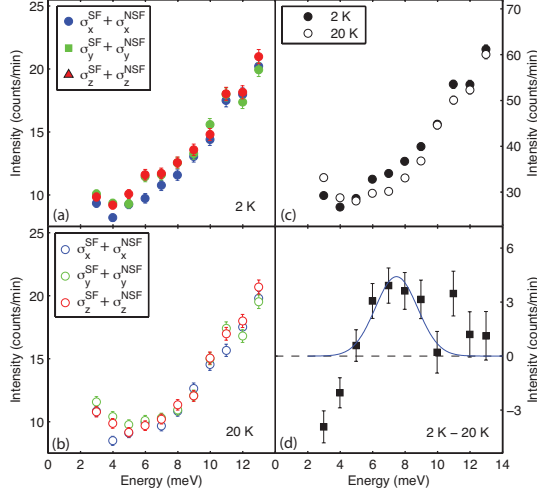


FIG. 3: (Color online) (a) Simulation of unpolarized energy scans using $\sigma_{\alpha}^{\text{SF}} + \sigma_{\alpha}^{\text{NSF}}$ with $\alpha = x, y, z$ at 2 K and (b) 20 K. The wave vector is fixed at $\mathbf{Q} = (0.5, 0.5, 1)$. (c) Unpolarized energy scan at $(1/2, 1/2, 1)$ below and above T_c obtained by adding all six channels together. (d) Temperature difference plot between 2 K and 20 K reveals a neutron spin resonance at $E = 7$ meV and negative scattering below 4 meV, very similar to the earlier unpolarized measurements on the same Ni-doping level¹⁶.

(Fig.1(a)). As a function of increasing Ni-doping x , the low-temperature crystal structure of $\text{BaFe}_{2-x}\text{Ni}_x\text{As}_2$ changes from orthorhombic to tetragonal with $a = b$ for $x \geq 0.1$ ^{11,12}. For this experiment, we coaligned ~ 15 g single crystals of $\text{BaFe}_{1.85}\text{Ni}_{0.15}\text{As}_2$ in the (H, H, L) scattering plane (with mosaicity 3° at full width half maximum) with a tetragonal unit cell for which $a = b = 3.96$ Å, and $c = 12.77$ Å. In this notation, the vector \mathbf{Q} in three-dimensional reciprocal space in \AA^{-1} is defined as $\mathbf{Q} = H\mathbf{a}^* + K\mathbf{b}^* + L\mathbf{c}^*$, where H , K , and L are Miller indices and $\mathbf{a}^* = \hat{\mathbf{a}}2\pi/a$, $\mathbf{b}^* = \hat{\mathbf{b}}2\pi/b$, $\mathbf{c}^* = \hat{\mathbf{c}}2\pi/c$ are reciprocal lattice vectors.

We carried out polarized inelastic neutron scattering experiments at the IN20 triple-axis spectrometer at the Institut Laue-Langevin in Grenoble, France. We used the Cryopad capability of the IN20 spectrometer in order to ensure that the sample was in a strictly zero magnetic field environment. This avoids errors due to flux inclusion and field expulsion in the superconducting phase of the sample. Polarized neutrons were produced using a focusing Heusler monochromator and analyzed using a focusing Heusler analyzer with a fixed final wave vector at $k_f = 2.662\text{\AA}^{-1}$. To facilitate easy comparison with previous polarized neutron scattering results³⁸, we define neutron polarization directions as x, y, z , with x parallel to \mathbf{Q} and y and z both perpendicular to \mathbf{Q} as shown in Fig. 1(b). Since neutron scattering is only sensitive to those magnetic scattering components perpendicular to the momentum transfer \mathbf{Q} , magnetic responses within the $y-z$ plane (M_y and M_z) can be measured. At a spe-

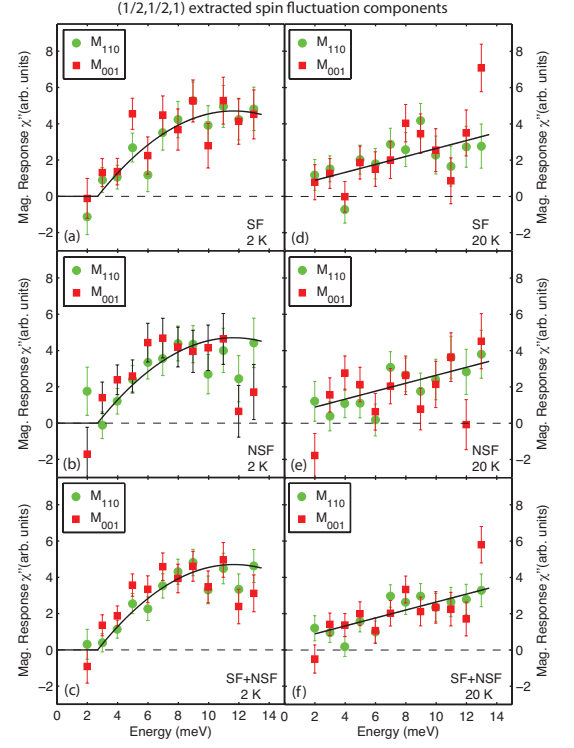


FIG. 4: (Color online) Neutron polarization analysis used to extract the in-plane (M_{110}) and out-of-plane M_{001} components of spin excitations in $\text{BaFe}_{1.85}\text{Ni}_{0.15}\text{As}_2$ from SF and NSF data in Fig. 2. M_{110} and M_{001} at 2 K are extracted from (a) SF, and (b) NSF data in Fig.2. (d,e) M_{110} and M_{001} at 20 K. The above analysis is based on the assumption that the background scattering for the x, y , and z spin polarizations are different (see eqs. (2) and (3)). However, if we assume that backgrounds are identical for different spin polarizations, we would obtain higher magnetic scattering intensity in the NSF channel compared with that of the SF channel at all measured temperatures and energies. At present, the microscopic origin of such a difference is unclear. (c) The combination of SF and NSF data at 2K. (f) The combination of SF and NSF data at 20K. These data reveal isotropic paramagnetic scattering at the probed energies and temperatures.

cific momentum and energy transfer, incident neutrons can be polarized along the x, y , and z directions, and the scattered neutrons can have polarizations either parallel (neutron nonspin flip or NSF, $\uparrow\uparrow$) or antiparallel (neutron spin flip or SF, $\uparrow\downarrow$) to the incident neutrons. Therefore, the six neutron scattering cross sections can be written as $\sigma_{\alpha}^{\text{NSF}}$ and $\sigma_{\alpha}^{\text{SF}}$, where $\alpha = x, y, z$ ^{35,38}. If we use M_{α} and N to denote the magnetic response and nuclear scattering, respectively, the neutron scattering cross sections $\sigma_{\alpha}^{\text{NSF}}$ and $\sigma_{\alpha}^{\text{SF}}$ are related to M_{α} and N via Eq. (1):

$$\begin{pmatrix} \sigma_x^{\text{SF}} \\ \sigma_y^{\text{SF}} \\ \sigma_z^{\text{SF}} \\ \sigma_x^{\text{NSF}} \\ \sigma_y^{\text{NSF}} \\ \sigma_z^{\text{NSF}} \end{pmatrix} = \begin{pmatrix} 1 & 1 & 0 \\ 0 & 1 & 0 \\ 1 & 0 & 0 \\ 0 & 0 & 1 \\ 1 & 0 & 1 \\ 0 & 1 & 1 \end{pmatrix} \times \begin{pmatrix} M_y \\ M_z \\ N \end{pmatrix} \quad (1)$$

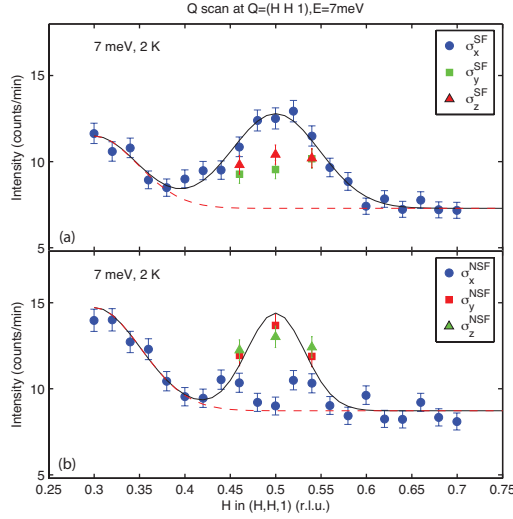


FIG. 5: (Color online) Constant-energy scans along the $[H, H, 1]$ direction at the resonance energy of $E = 7$ meV at 2 K for different neutron polarization directions. (a) Neutron SF scattering cross sections for the x , y , and z polarization directions. (b) NSF scattering cross sections. A clear peak is seen at $\mathbf{Q} = (0.5, 0.5, 1)$ in the σ_x^{SF} channel that is absent in the σ_x^{NSF} channel, thus confirming the magnetic nature of the resonance.

In a real experiment, neutron polarization is not 100% and there are also neutron spin independent backgrounds (nuclear-spin incoherent scattering and general instrumental background). Since neutron SF and NSF scattering processes have identical instrumental setups and only the spin directions of the incident neutrons are changed, we assume constant backgrounds of B_1 , B_2 , B_3 for neutron polarizations in the x , y , and z directions, respectively. We have measured the neutron flipping ratios R for all three neutron polarizations, and found them to be independent of neutron polarization directions within the errors of our measurements. By considering finite flipping ratio and assume that instrumental backgrounds for different neutron polarizations are slightly different, we have

$$\begin{pmatrix} \sigma_x^{\text{SF}} - B_1 \\ \sigma_y^{\text{SF}} - B_2 \\ \sigma_z^{\text{SF}} - B_3 \\ \sigma_x^{\text{NSF}} - B_1 \\ \sigma_y^{\text{NSF}} - B_2 \\ \sigma_z^{\text{NSF}} - B_3 \end{pmatrix} = \frac{1}{R+1} \begin{pmatrix} R & R & 1 \\ 1 & R & 1 \\ R & 1 & 1 \\ 1 & 1 & R \\ R & 1 & R \\ 1 & R & R \end{pmatrix} \times \begin{pmatrix} M_y \\ M_z \\ N \end{pmatrix}, \quad (2)$$

where the flipping ratio R is measured by the leakage of NSF nuclear Bragg peaks into the magnetic SF channel $R = \sigma_{\text{Bragg}}^{\text{NSF}} / \sigma_{\text{Bragg}}^{\text{SF}} \approx 14$. The magnetic moments M_y and M_z can be extracted from Eq.(2) via

$$\begin{cases} \sigma_x^{\text{SF}} - \sigma_y^{\text{SF}} + B_1 = \sigma_y^{\text{NSF}} - \sigma_x^{\text{NSF}} - B_1 = cM_y, \\ \sigma_x^{\text{SF}} - \sigma_z^{\text{SF}} + B_2 = \sigma_z^{\text{NSF}} - \sigma_x^{\text{NSF}} - B_2 = cM_z \end{cases} \quad (3)$$

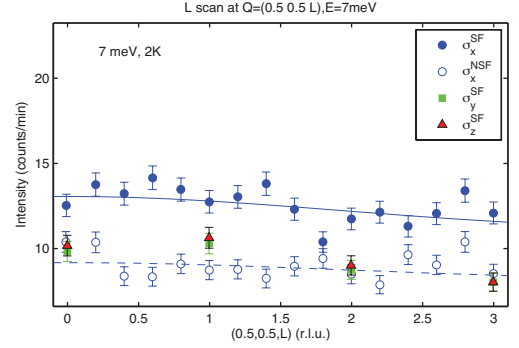


FIG. 6: (Color online) Constant-energy scans along $(0.5, 0.5, L)$ at the resonance energy of $E = 7$ meV. The σ_x^{SF} and σ_x^{NSF} data show no L dependence. The solid and dashed lines show the expected magnetic scattering intensity assuming an Fe^{2+} form factor.

where $c = (R-1)/(R+1)$, and B_1, B_2 are constant backgrounds. By measuring all six NSF and SF neutron scattering cross sections, we can unambiguously determine M_y and M_z . To estimate the in-plane and out-of-plane components of the magnetic scattering M_{110} and M_{001} , we note that $M_{110} = M_{1\bar{1}0} \equiv M_z$ due to the tetragonal symmetry of the system. Therefore, M_{001} can be calculated using $M_y = M_{110} \sin^2 \theta + M_{001} \cos^2 \theta$. This allows a complete determination of the temperature and energy dependence of M_{110} and M_{001} .

III. RESULTS

In previous polarized neutron scattering experiments performed on optimally doped $\text{BaFe}_{1.9}\text{Ni}_{0.1}\text{As}_2$ ³⁸, the in-plane (M_{110}) and out-of-plane (M_{001}) magnetic fluctuations are gapless and approximately isotropic in the normal state above T_c . Upon entering the superconducting state, the M_{110} spectra re-arrange with a spin gap below $E = 2$ meV and a resonance peak near $E = 7$ meV. On the other hand, the M_{001} spectra peak near $E = 4$ meV and have a smaller spin gap (Fig. 3 in Ref. 38). Figures 2(a)-2(d) show all six constant- \mathbf{Q} scattering cross sections $\sigma_{x,y,z}^{\text{SF}}$ and $\sigma_{x,y,z}^{\text{NSF}}$ taken at the AF wave vector $\mathbf{Q} = (1/2, 1/2, 1)$ below and above T_c . For SF scattering, σ_y^{SF} is approximately equal to σ_z^{SF} at 2 K and 20 K, but both σ_y^{SF} and σ_z^{SF} are smaller than σ_x^{SF} (Figs. 2(a) and 2(c)). For the NSF scattering, the situation is similar except that σ_x^{NSF} is smaller than σ_y^{NSF} and σ_z^{NSF} (Figs. 2(b) and 2(d)). These results indicate the presence of paramagnetic scattering, since for purely nuclear scattering there would be no difference between the scattering from different neutron polarizations ($\sigma_x^{\text{SF}} = \sigma_y^{\text{SF}} = \sigma_z^{\text{SF}}$)³⁵.

In a previous unpolarized neutron scattering experiment performed on $\text{BaFe}_{1.85}\text{Ni}_{0.15}\text{As}_2$, a neutron spin resonance was observed near $E = 6$ meV in the superconducting state, found by taking a temperature difference between constant- \mathbf{Q} scans at $(0.5, 0.5, 1)$ r.l.u.¹⁶. Before

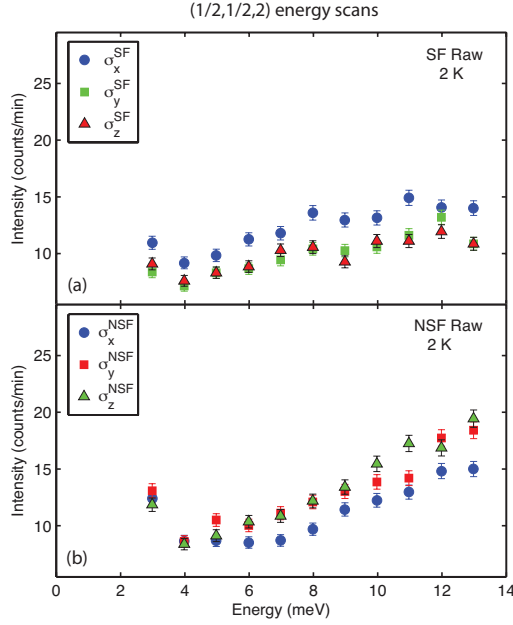


FIG. 7: (Color online) Constant- Q scans at $\mathbf{Q} = (0.5, 0.5, 2)$ at 2 K. (a) The three neutron SF scattering energy scans below T_c , marked as $\sigma_{x,y,z}^{\text{SF}}$. (b) Identical scans in the neutron NSF channel, marked as $\sigma_{x,y,z}^{\text{NSF}}$.

determining the possible magnetic anisotropy from neutron polarization analysis, we note from Eq. (2) that $\sigma_x^{\text{SF}} + \sigma_x^{\text{NSF}} = M_y + M_z + N + 2B_1$, $\sigma_y^{\text{SF}} + \sigma_y^{\text{NSF}} = M_y + M_z + N + 2B_2$, and $\sigma_z^{\text{SF}} + \sigma_z^{\text{NSF}} = M_y + M_z + N + 2B_3$ are the scattering cross sections for an unpolarized neutron scattering experiment. Assuming the background scattering has no temperature dependence across T_c , the temperature difference data of $\sigma_{\alpha}^{\text{SF}} + \sigma_{\alpha}^{\text{NSF}}$ should recover unpolarized neutron scattering results¹⁶. Figures 3(a) and 3(b) show the sum of the raw data $\sigma_{\alpha}^{\text{SF}} + \sigma_{\alpha}^{\text{NSF}}$ above and below T_c , respectively for $\alpha = x, y$ and z . Figure 3(c) plots the sum of all six scattering cross sections $\sigma_{x,y,z}^{\text{SF}}$ and $\sigma_{x,y,z}^{\text{NSF}}$ at $\mathbf{Q} = (1/2, 1/2, 1)$ below and above T_c . The temperature difference in Fig. 3(d) clearly shows a resonant feature at $E = 7$ meV, consistent with earlier unpolarized neutron scattering results¹⁶.

To extract any possible anisotropy of the resonance and normal state spin excitations, we use $\sigma_{\alpha}^{\text{SF}}$ and $\sigma_{\alpha}^{\text{NSF}}$ with Eq. (3) to independently determine M_y and M_z . Since M_z is equal to M_{110} and $M_y = M_{110} \sin^2 \theta + M_{001} \cos^2 \theta$, M_{110} and M_{001} can be independently calculated from either $\sigma_{\alpha}^{\text{SF}}$ or $\sigma_{\alpha}^{\text{NSF}}$. One can then calculate the imaginary part of the dynamic susceptibility $\chi''(Q, \omega)$ via $\chi''(Q, \omega) = [1 - \exp(-\hbar\omega/k_B T)]S(Q, \omega)$, where $S(Q, \omega) = M_{110}$ or M_{001} , and $E = \hbar\omega$. Figures 4(a)-4(d) summarize results for $\chi''_{110}(Q, \omega)$ and $\chi''_{001}(Q, \omega)$ at the AF wave vector $Q = (0.5, 0.5, 1)$ in the superconducting and normal states, respectively. The $\chi''_{110}(Q, \omega)$ and $\chi''_{001}(Q, \omega)$ results in Figs. 4(a) and 4(b) are obtained using $\sigma_{\alpha}^{\text{SF}}$, while the similar results shown in Figs. 4(c) and 4(d) are independent calculations us-

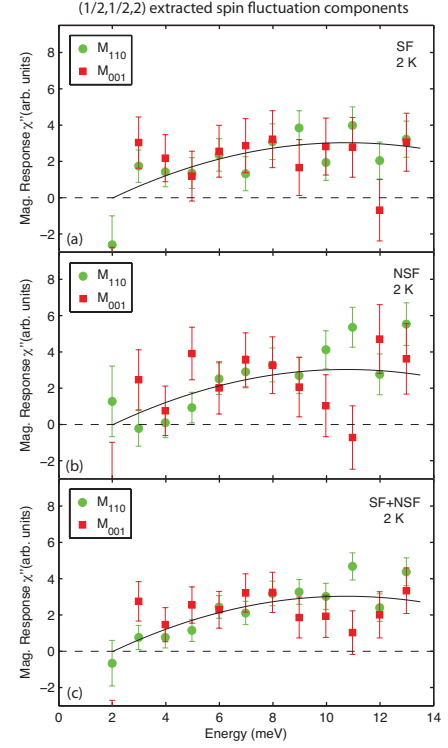


FIG. 8: (Color online) Constant- Q scans at $\mathbf{Q} = (0.5, 0.5, 2)$ at 2 K. The in-plane (M_{110}) and out-of-plane (M_{001}) magnetic response extracted from the (a) SF data, and (b) NSF data, respectively; (c) The combination of SF and NSF data at 2 K shows no difference between the two magnetic moment components, indicating isotropic paramagnetic scattering.

ing $\sigma_{\alpha}^{\text{NSF}}$. These results are identical to within the errors of the measurements. Figures 4(c) and 4(d) show combined SF+NSF results for $\chi''_{110}(Q, \omega)$ and $\chi''_{001}(Q, \omega)$ to improve the statistics. In the normal state at 20 K, $\chi''_{110}(Q, \omega)$ and $\chi''_{001}(Q, \omega)$ are identical and increase linearly with increasing energy (Fig. 4(f)). At low temperatures ($T = 2$ K, a spin gap is present below $E \approx 3$ meV and a broad resonance is apparent near $E \approx 7$ meV. $\chi''_{110}(Q, \omega)$ and $\chi''_{001}(Q, \omega)$ are again identical to within the errors of our measurements. Therefore, there is no observable magnetic anisotropy of the spin excitations of overdoped $\text{BaFe}_{1.85}\text{Ni}_{0.15}\text{As}_2$ in both the normal and superconducting states at $\mathbf{Q} = (0.5, 0.5, 1)$.

Figures 5(a) and 5(b) show constant-energy scans at the resonance energy along $(H, H, 1)$ for $\sigma_{\alpha}^{\text{SF}}$ and $\sigma_{\alpha}^{\text{NSF}}$. While the SF scattering σ_x^{SF} shows a clear peak centered at the AF wave vector $\mathbf{Q} = (0.5, 0.5, 1)$ (Fig. 5(a)), the NSF scattering σ_x^{NSF} (Fig. 5(b)) is featureless near $\mathbf{Q} = (0.5, 0.5, 1)$. This suggests that the resonance peak above the background in Fig. 5(a) is entirely magnetic in origin. If the resonance is purely isotropic paramagnetic scattering, one would expect $\sigma_x^{\text{SF}} - B_1 \approx 2(\sigma_y^{\text{SF}} - B_2) \approx 2(\sigma_z^{\text{SF}} - B_3)$ and $(\sigma_y^{\text{NSF}} - B_2) \approx (\sigma_z^{\text{NSF}} - B_3)$. Inspection of Figs. 5(a) and 5(b) reveal that this is indeed the case, thus confirming the isotropic nature of the magnetic

resonance.

To determine whether the spin excitations at the resonance energy exhibit any c -axis modulation in intensity, we carried out constant-energy scans along $(0.5, 0.5, L)$ in the superconducting state at $E = 7$ meV. As one can see in Fig. 6, the magnetic scattering intensity decreases smoothly with increasing L , consistent with the expected magnetic intensity reduction due to the Fe^{2+} form factor (solid line). There is no evidence for a L -axis modulation of the magnetic scattering.

Finally, to see whether the isotropic magnetic scattering near the AF wave vector $\mathbf{Q} = (0.5, 0.5, 1)$ is independent of the c -axis momentum transfer, we carried out $\sigma_{\alpha}^{\text{SF}}$ and $\sigma_{\alpha}^{\text{NSF}}$ constant- Q scans in the superconducting state at $\mathbf{Q} = (0.5, 0.5, 2)$ (Fig. 7). Similar to the data in Fig. 2, the SF scattering σ_x^{SF} is larger than σ_y^{SF} and σ_z^{SF} (Fig. 7(a)), while the NSF scattering σ_x^{NSF} is smaller than σ_y^{NSF} and σ_z^{NSF} . Using this raw data shown in Fig. 7, we are able to obtain the energy dependence of $\chi''_{110}(Q, \omega)$ and $\chi''_{001}(Q, \omega)$ at $\mathbf{Q} = (0.5, 0.5, 2)$ as shown in Figs. 8(a) and 8(b). Consistent with the constant- Q scans at $\mathbf{Q} = (0.5, 0.5, 1)$, we find isotropic magnetic scattering at $\mathbf{Q} = (0.5, 0.5, 2)$. Figure 8(c) shows the energy dependence of $\chi''_{110}(Q, \omega)$ and $\chi''_{001}(Q, \omega)$ obtained by combining the SF and NSF scattering data in Figs. 8(a) and 8(b). Similar to Fig. 4(c), a spin gap is present below $E = 3$ meV and $\chi''_{110}(Q, \omega)$ and $\chi''_{001}(Q, \omega)$ increase with increasing energy. Therefore, spin excitations in overdoped $\text{BaFe}_{1.85}\text{Ni}_{0.15}\text{As}_2$ are isotropic below and above T_c at all energies probed.

IV. DISCUSSION AND CONCLUSIONS

In previous polarized neutron scattering experiments on optimally electron-doped $\text{BaFe}_{1.9}\text{Ni}_{0.15}\text{As}_2$, $\chi''_{110}(Q, \omega)$ and $\chi''_{001}(Q, \omega)$ at $\mathbf{Q} = (0.5, 0.5, 1)$ were found to have peaks near $E = 7$ and 4 meV, respectively, in the superconducting state³⁸. These results were interpreted as being due to the presence of spin-orbital/lattice coupling³⁸. In a recent polarized neutron scattering work

on the AF parent compound BaFe_2As_2 , it was found that in-plane polarized magnons exhibit a larger single iron anisotropy gap than the out-of-plane polarized ones⁴⁰. This means that $\chi''_{110}(Q, \omega)$ has a larger gap than $\chi''_{001}(Q, \omega)$ at $\mathbf{Q} = (0.5, 0.5, 1)$ in the AF ordered state, where the Fe moments are locked to the a -axis of the orthorhombic structure^{44–46} [along the $[110]$ direction in our tetragonal notation].

From the electronic phase diagram of $\text{BaFe}_{2-x}\text{Ni}_x\text{As}_2$ in Fig. 1(a), we see that although the optimally electron-doped $\text{BaFe}_{1.9}\text{Ni}_{0.1}\text{As}_2$ has tetragonal structure with no static AF order¹², it is very close to that region of the phase diagram where incommensurate static AF order coexists with superconductivity¹¹. This suggests that the observed anisotropy between the in-plane ($\chi''_{110}(Q, \omega)$) and out-of-plane ($\chi''_{001}(Q, \omega)$) dynamic susceptibility in tetragonal superconducting $\text{BaFe}_{1.9}\text{Ni}_{0.1}\text{As}_2$ ³⁸ may have the same microscopic origin as the spin wave anisotropy gaps in the AF orthorhombic BaFe_2As_2 ⁴⁰. If this is indeed the case, the resonance is only weakly anisotropic near optimal superconductivity, and becomes isotropic in the electron over-doped $\text{BaFe}_{1.9}\text{Ni}_{0.15}\text{As}_2$. Therefore, these results suggest that the resonance in electron over-doped $\text{BaFe}_{2-x}\text{Ni}_x\text{As}_2$ is mostly consistent with the singlet-triplet excitations of electron Cooper pairs. The observed spin excitation anisotropy in optimally doped $\text{BaFe}_{2-x}\text{Ni}_x\text{As}_2$ is likely due to single iron anisotropy of spin waves in the parent compound, and suggests that such anisotropy is present even for samples with tetragonal structure. Thus, the strong spin-orbital-lattice coupling in electron-doped $\text{BaFe}_{1.9}\text{Ni}_{0.1}\text{As}_2$ is important for samples up to optimal superconductivity, and becomes less important for the overdoped regime.

V. ACKNOWLEDGEMENTS

The work at UTK is supported by the U.S. NSF-DMR-1063866. Work at IOP is supported by the MOST of China 973 programs (2012CB821400, 2011CBA00110) and NSFC-11004233.

-
- ¹ Y. Kamihara, T. Watanabe, M. Hirano, and H. Hosono, J. Am. Chem. Soc. **130**, 3296 (2008).
 - ² M. Rotter, M. Tegel, and D. Johrendt, Phys. Rev. Lett. **101**, 107006 (2008).
 - ³ L. J. Li, Y. K. Luo, Q. B. Wang, H. Chen, Z. Ren, Q. Tao, Y. K. Li, X. Lin, M. He, Z. W. Zhu, G. H. Cao, and Z. A. Xu, New J. Phys. **11**, 025008 (2009).
 - ⁴ I. I. Mazin, D. J. Singh, M. D. Johannes and M. H. Du, Phys. Rev. Lett. **101**, 057003 (2008).
 - ⁵ M. M. Korshunov and I. Eremin, Phys. Rev. B **78**, 140509(R) (2008).
 - ⁶ T. A. Maier and D. J. Scalapino, Phys. Rev. B **78**, 020514(R) (2008).
 - ⁷ T. A. Maier, S. Graser, D. J. Scalapino and P. Hirschfeld,

- Phys. Rev. B **79**, 134520 (2009).
- ⁸ K. Seo, C. Fang, B. A. Bernevig and J. Hu, Phys. Rev. B **79**, 235207 (2009).
- ⁹ C. de la Cruz, Q. Huang, J. W. Lynn, J. Li, W. Ratcliff II, J. L. Zarestky, H. A. Mook, G. F. Chen, J. L. Luo, N. L. Wang, and P. Dai, Nature (London) **453**, 899 (2008).
- ¹⁰ C. Lester, Jiun-Haw Chu, J. G. Analytis, S. C. Capelli, A. S. Erickson, C. L. Condon, M. F. Toney, I. R. Fisher, and S. M. Hayden, Phys. Rev. B **79**, 144523 (2009).
- ¹¹ Huiqian Luo, Ru Zhang, M. Laver, Z. Yamani, Meng Wang, Xingye Lu, M. Y. Wang, Yanchao Chen, Shiliang Li, Sung Chang, J. W. Lynn, and Pengcheng Dai, arXiv: 1203.2759.
- ¹² S. Chi, A. Schneidewind, J. Zhao, L. W. Harriger, L. Li,

- Y. Luo, G. Cao, Z. Xu, M. Loewenhaupt, J. Hu and P. Dai, Phys. Rev. Lett. **102**, 107006 (2009).
- ¹³ M. D. Lumsden, A. D. Christianson, D. Parshall, M. B. Stone, S. E. Nagler, G. J. MacDougall, H. A. Mook, K. Lokshin, T. Egami, D. L. Abernathy, E. A. Goremychkin, R. Osborn, M. A. McGuire, A. S. Sefat, R. Jin, B. C. Sales and D. Mandrus, Phys. Rev. Lett. **102**, 107005 (2009).
 - ¹⁴ S. Li, Y. Chen, S. Chang, J. W. Lynn, L. Li, Y. Luo, G. Cao, Z. Xu and P. Dai, Phys. Rev. B **79**, 174527 (2009).
 - ¹⁵ D. S. Inosov, J. T. Park, P. Bourges, D. L. Sun, Y. Sidis, A. Schneidewind, K. Hradil, D. Haug, C.T. Lin, B. Keimer and V. Hinkov, Nat. Phys. **6**, 178 (2010).
 - ¹⁶ M. Wang, H. Luo, J. Zhao, C. Zhang, M. Wang, K. Marty, S. Chi, J. W. Lynn, A. Schneidewind, S. Li and P. Dai, Phys. Rev. B **81**, 174524 (2010).
 - ¹⁷ J. T. Park, D. S. Inosov, A. Yaresko, S. Graser, D. L. Sun, Ph. Bourges, Y. Sidis, Yuan Li, J.-H. Kim, D. Haug, A. Ivanov, K. Hradil, A. Schneidewind, P. Link, E. Faulhaber, I. Glavatsky, C. T. Lin, B. Keimer, and V. Hinkov, Phys. Rev. B **82**, 134503 (2010).
 - ¹⁸ D. S. Inosov, J. T. Park, A. Charnukha, Yuan Li, A. V. Boris, B. Keimer, and V. Hinkov, Phys. Rev. B **83**, 214520 (2011).
 - ¹⁹ J. Rossat-Mignod, L. P. Regnault, C. Vettier, P. Bourges, P. Burlet, J. Bossy, J. Y. Henry and G. Lapertot, Physica C (Amsterdam) **185**, 86 (1991).
 - ²⁰ H. A. Mook, G. Aeppli and T. E. Mason and T. Armstrong, Phys. Rev. Lett. **70**, 3490 (1993).
 - ²¹ H. F. Fong, B. Keimer, D. Reznik, D. L. Milius and I. A. Aksay, Phys. Rev. B **54**, 6708 (1996).
 - ²² Pengcheng Dai, H. A. Mook, R. D. Hunt and F. Doğan, Phys. Rev. B **63**, 054525 (2001).
 - ²³ S. D. Wilson, P. Dai, S. Li, S. Chi, H. J. Kang and J. W. Lynn, Nature (London) **442**, 59 (2006).
 - ²⁴ N. Metoki, Y. Haga, Y. Koike and Y. Ōnuki, Phys. Rev. Lett. **80**, 5417 (1998).
 - ²⁵ C. Stock, C. Broholm, J. Hudis, H. J. Kang and C. Petrovic, Phys. Rev. Lett. **100**, 087001 (2008).
 - ²⁶ H. A. Mook *et al.*, Phys. Rev. Lett. **104**, 187002 (2010).
 - ²⁷ Y. Qiu *et al.*, Phys. Rev. Lett. **103**, 067008 (2009).
 - ²⁸ L. W. Harriger, O. J. Lipscombe, C. L. Zhang, H. Q. Luo, M. Wang, K. Marty, M. D. Lumsden, and Pengcheng Dai, Phys. Rev. B **85**, 014510 (2012).
 - ²⁹ M. Eschrig, Adv. Phys. **55**, 47 (2006).
 - ³⁰ Pengcheng Dai, H. A. Mook, G. Aeppli, S. M. Hayden, and F. Dogan, Nature (London) **406**, 965 (2000).
 - ³¹ J. Wen, G. Xu, Z. Xu, Z.W. Lin, Q. Li, Y. Chen, S. Chi, G. Gu, and J. M. Tranquada, Phys. Rev. B **81**, 100513(R) (2010).
 - ³² S. L. Li, X. Y. Lu, M. Wang, H. Q. Luo, M. Y. Wang, C. L. Zhang, E. Faulhaber, L.-P. Regnault, D. Singh, and Pengcheng Dai, Phys. Rev. B **84**, 024518 (2011).
 - ³³ C. Stock, C. Broholm, Y. Zhao, F. Demmel, H.J. Kang, K. C. Rule, and C. Petrovic, arXiv: 1203.2189v1.
 - ³⁴ Jun Zhao, L.-P. Regnault, C. L. Zhang, M. Y. Wang, Z. C. Li, F. Zhou, Z. X. Zhao, C. Fang, J. P. Hu, and Pengcheng Dai, Phys. Rev. B **81**, 180505(R) (2010).
 - ³⁵ R. M. Moon, T. Riste, and W. C. Koehler, Phys. Rev. **181**, 920 (1969).
 - ³⁶ N. S. Headings, S. M. Hayden, J. Kulda, N. Hari Babu, and D. A. Cardwell, Phys. Rev. B **84**, 104513 (2011).
 - ³⁷ D. Coffey, T. M. Rice, and F. C. Zhang, Phys. Rev. B **44**, 10112 (1991).
 - ³⁸ O. J. Lipscombe, L. W. Harriger, P. G. Freeman, M. Enderle, C. L. Zhang, M. Y. Wang, T. Egami, J. P. Hu, T. Xiang, M. R. Norman, and Pengcheng Dai, Phys. Rev. B **82**, 064515 (2010).
 - ³⁹ P. Babkevich, B. Roessli, S. N. Gvasaliya, L.-P. Regnault, P. G. Freeman, E. Pomjakushina, K. Conder, and A. T. Boothroyd, Phys. Rev. B **83**, 180506(R) (2011).
 - ⁴⁰ N. Qureshi, P. Steffens, S. Wurmehl, S. Aswartham, B. Büchner, and M. Braden, arXiv:1201.2332v1.
 - ⁴¹ Jun Zhao, D. X. Yao, S. Li, T. Hong, Y. Chen, S. Chang, W. Ratcliff II, J. W. Lynn, H. A. Mook, G. F. Chen, J. L. Luo, N. L. Wang, E.W. Carlson, J. P. Hu, and P. Dai, Phys. Rev. Lett. **101**, 167203 (2008).
 - ⁴² K. Matan, R. Morinaga, K. Iida, and T. J. Sato, Phys. Rev. B **79**, 054526 (2009).
 - ⁴³ Y. C. Chen, X. Y. Lu, M. Wang, H. Q. Luo, and S. L. Li, S. L., Supercond. Sci. Technol. **24**, 065004 (2011).
 - ⁴⁴ Q. Huang, Y. Qiu, W. Bao, M. A. Green, J. W. Lynn, Y. C. Gasparovic, T. Wu, G. Wu and X. H. Chen, Phys. Rev. Lett. **101**, 257003 (2008).
 - ⁴⁵ J. Zhao, W. Ratcliff, J. W. Lynn, G. F. Chen, J. L. Luo, N. L. Wang, J. Hu and P. Dai, Phys. Rev. B **78**, 140504(R) (2008).
 - ⁴⁶ A. I. Goldman, D. N. Argyriou, B. Ouladdiaf, T. Chatterji, A. Kreyssig, S. Nandi, N. Ni, S. L. Bud'ko, P. C. Canfield and R. J. McQueeney, Phys. Rev. B **78**, 100506(R) (2008).